International Journal of Offshore and Coastal Engineering
Vol.6 | No. 2 | pp. 81 – 90 | November 2022
e-ISSN: 2580-0914


Submitted: July 15, 2022 | Revised: September 9, 2022| Accepted: October 11, 2022

# Tension Leg Rectangular Fish Cage Motion Analysis in Regular and Random Waves

Raditya Danu Riyanto [a*], Yuni Ari Wibowo[b] and Mochammad Ramzi[c]

[a)] Department of Ocean Engineering, Institut Teknologi Sepuluh Nopember, Surabaya 60111, Indonesia
[b)] Polytechnics of Marine and Fisheries, Pangandaran, Indonesia
[c)] Groot Ship Design, Groningen, Netherlands
*Corresponding author: radityadanu@its.ac.id

## ABSTRACT

*This paper uses an analytical method to examine the motion of a Tension Leg Fish Cage (TLFC) in regular and random waves. TLFC is a conceptual design of a fish cage based on the Tension Leg Platform (TLP) working principle that is usually used in deep water offshore oil and gas exploration. The idea of providing a safe environment to combine ecotourism and fish farming in a single platform led us to perform an analytical calculation to assess the possibility of using the TLP concept in fish farming. A preliminary conceptual design of TLFC using an HDPE floater with steel cable tendon is presented. The analytical calculation of the response amplitude operator for surge and heave motion is presented using linear airy wave theory with head seas encountering angle. This paper also presents the calculation of TLFC surge and heave motion under random wave loads. The random wave spectra used in this paper are JONSWAP and ISSC spectra. The result shows that the surge and heave motion response of TLFC is relatively small and, therefore, can be analyzed further with more detailed consideration. It is admitted that HDPE is a brittle material that cannot sustain any long period of constant tension. Hence the optimum tendon-floater connection for the structure is subject to further research.*

**Keywords:** *Tension Leg Rectangular Fish Cage, surge, heave, Response Amplitude Operator (RAO).*

## 1. INTRODUCTION

From a global perspective, the demand for fisheries products increasing in the past few years [1]. However, while some species recover more quickly than others, it is clear that marine fish availability is dangerously decreasing [2]. In Indonesia, the capture fisheries are in a very dire condition where the production decreased rapidly until only not more than 0.1 million tons of fish were captured in 2018, as shown in Figure 1 [3]. Not only because of overfishing but the severe habitat destruction is also caused by irresponsible acts of fishing, e.g., poisons and explosives for fish catching. Illegal fishing by trawlers from neighboring countries also worsens the situation [4]. Based on FAO's data (Food and Agricultural Organization of the United Nations), aquaculture fisheries production increased rapidly from 2005 onwards, outnumbering the capture fisheries hundreds of folds. Figure 1 shows that in 2015, aquaculture reached nearly 11.3 million tons, while the capture fisheries only produced 0.04 million tons of fisheries. From this fact, we can see that the future of Indonesian fisheries supply is from aquaculture.

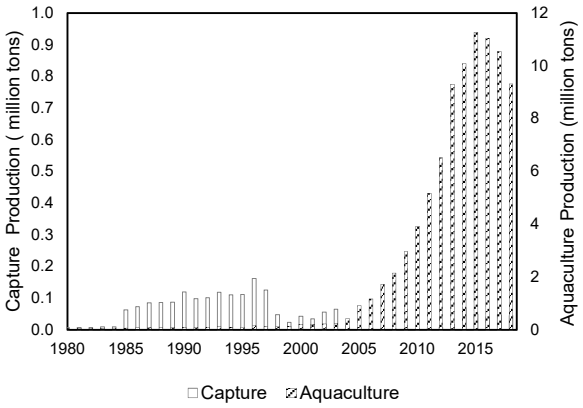


Figure 1. Capture and aquaculture fisheries production of the Republic of Indonesia [3].

Aquaculture production comes from several sources, namely inland and marine aquaculture. The inland aquaculture consists of freshwater and brackishwater aquaculture. As shown in Figure 2, most aquaculture production came from inland waters. The peak production in 2017 was when inland aquaculture produced up to 5.5 million fisheries products. Most inland water production is generated from traditional aquaculture, with the typical

example in Figure 3, where freshwater carp fishes are harvested [5]. However, traditional inland aquaculture has shown a decreasing trend since 2015. It is subject to a further decrease to 2 million tons in three years due to the massive land conversion from an agricultural region to housing and industrial estates [6].

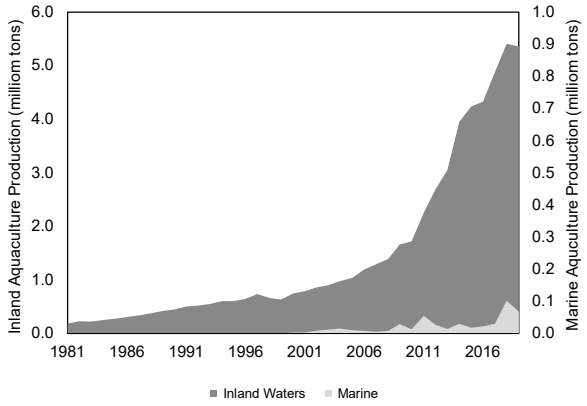


Figure 2. Aquaculture production by the cultural environment of the Republic of Indonesia [3].

The production decrease of inland waters aquaculture and the depleting capture fisheries brings the effort towards marine aquaculture. In the coastal region, marine aquaculture will interfere with many stakeholders, such as marine traffic, industrial pollution, and tourism objects. Hence the future of aquaculture will go further off the coast, with lower interference and higher nutrient assimilation capacity [7].

Figure 3. Traditional inland water fish cage [5]

Recently, an effort to accumulate existing offshore aquaculture technologies has been performed and presented in [8] and categorized the existing offshore aquaculture structures installed worldwide into categories as described in Table 1.

Table 1. Types of offshore aquaculture structure designs and its features (summarized from [8])

| Types of fish cages | Material | Capital cost |
|---|---|---|
| Floating flexible | Flexible hose | Low |
| Floating rigid | Steel | High |
| Semi-submersible rigid | Steel | High |
| Semi-submersible flexible | Tension leg and flexible hose | Low |
| Submerged | Steel, concrete | High |

This paper investigates another alternative to offshore aquaculture platforms. The concept proposed in this paper is the hybrid Tension Leg Fish Cage (TLFC), with an HDPE-based floater moored to pre-tensioned tendon and mooring blocks. This configuration is expected to provide a safe environment on the floater structures to accommodate research ecotourism and relatively pleasant motion response when subjected to the wave loads [9]. The TLFC is inspired by a Tension Leg Platform (TLP), which is usually fabricated for the offshore oil and gas industry. A TLP is a vertically connected unsinkable compliant structural system that the buoyancy of the platform that creates tension in the anchoring system. The TLP is generally designed to serve several functional roles and offshore oil and gas usage. It is mainly used for deep water applications [10].

A Tension Leg Platform (TLP) is a buoyant floater unit connected to a fixed foundation (or piles) by pre-tensioned tendons. The tendons usually are parallel, near-vertical elements, acting in tension, which typically restrains the motions of the TLP in heave, roll, and pitch. The platform is usually compliant in the surge, sway, and yaw [9].

This paper demonstrates the analytical methodology to calculate the motion of TLFC in regular and random waves for surge and heave motion from head seas. We investigate the effect of draft variation of TLFC floater on its surge response. This paper also investigates several parameters concerning the draft variation of TLFC, namely tether tension force, excitation force, Response Amplitude Operator (RAO), and Spectral Response from JONSWAP and ISSC spectra. The result of this investigation will be the basis of further TLFC development for a more detailed design.

## 2. METHOD

The analytical calculation approach of TLFC, considering its mass, damping, and stiffness formulation, is performed in this paper. The floater motion is considered rigid body dynamics [10] and can be expressed as:

$$\{\mathbf{M}+\mathbf{M_A}\}\ddot{\boldsymbol{u}}+\{\boldsymbol{C_v}\}\dot{\boldsymbol{u}}+\{\mathbf{K}+\mathbf{K_m}\}\boldsymbol{u}=\{\mathbf{F}\}(\mathbf{t}) \quad (1)$$

Where $\ddot{u}$, $\dot{u}$, and $u$ are the vectors of acceleration, velocity, and displacement in corresponding motion ($x$ for surge and $z$ for heave). $\mathrm{M}+\mathrm{M_A}$ is the component of physical mass and added mass. $C_\mathrm{v}$ is the component of hydrodynamics damping. $\mathrm{K}+\mathrm{K_m}$ is the addition of hydrostatic stiffness and tendon stiffness. $\{F\}(t)$ is the excitation force generated by the wave loads on the TLFC floater. In the analysis performed in this paper, we apply linear airy wave loads, with several assumptions listed below [11]:

1. Wave amplitude is considered small to its length and the water depth.
2. Constant water depth.
3. Nonviscous, incompressible water.

In this paper, the water depth is assumed as Class 2 off-coast farming as described by [12] and set to a constant water depth of 15 m. Figure 4 below explains the methodology to calculate the TLFC motion. The analysis starts with calculating TLFC displacement and added mass, and then the motion stiffness is calculated, assuming the predetermined tendon tension. The mass and stiffness results are then utilized to calculate its natural period in the corresponding motion.

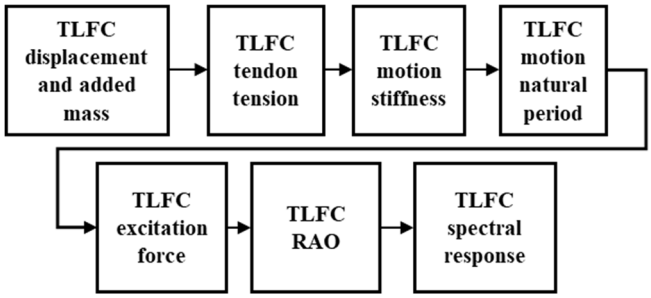

Figure 4. TLP surge motion analysis flowchart

The excitation force, the right-hand part of equation (1), is then calculated. The Response Amplitude Operator (RAO) can be determined after we solve equation (1) to determine the motion characteristics in regular waves. Furthermore, we determine the wave spectra using JONSWAP and ISSC Equation to predict the TLFC motion in random waves.

## 3. TLFC DESIGN CONCEPT

### 3.1 Dimension and major body parts

The floater adopts the generic Tension Leg Platform model with a similar dimension between length and beam. There are four columns at each side of the rectangle connected with a pontoon at each side, resulting in every four columns and pontoons. The TLFC floater dimension used in this analysis is described in Table 2 below. There are four tendons, each connecting one column to the fixed foundation laying in the seabed. In this paper, we will investigate the use of steel cable tendons and examine its efficacy by the motion response. The TLFC tendon properties are described in Table 3.

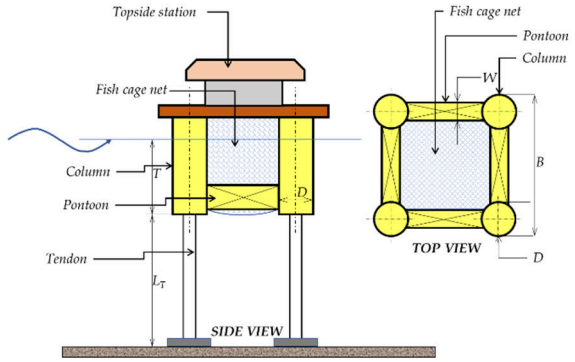

Figure 5. TLP Dimension

Table 2. Pontoon and Column Dimension of TLFC

| Pontoon Dimension (m) | | Column Dimension (m) | |
|---|---|---|---|
| Length | 8 | Diameter | 2.0 |
| Breadth | 2 | Height | 6.0 |
| Height | 1 | Free Floating Draft | 3.5 |
| | | Maximum Draft | 5.0 |

HDPE (High-Density Polyethylene) is the floater material for pontoons and columns with specific gravity weight ton/m$^3$. The topside station consists of fishing gear, station building, and communication apparatus. There are also mechanical and electrical as well as instrumental apparatus. The station building consists of marine-grade wood used for deck flooring panels with steel beams as girders. The structural details are not in this paper's scope. Hence only important points for gravity loads are described in Table 4 below. The assumption of the fish stock load is from [8], taking the one-third of the Semi-submersible (*Refa*) tension leg with full capacity, considering the total breadth TLFC is only one-third of the Refa model diameter.

Table 3. TLFC Tendon Properties

| Description | Measurement | Unit |
|---|---|---|
| Tendon Length | 15 | m |
| Tendon OD (Outer Diameter) | 600 | mm |
| Tendon WT (Wall Thickness) | 75 | mm |
| Young's Modulus € | 210 | MPa |
| Allowable Tendon Stress ($T_F$) | 50 | MPa |
| Number of tendons | 4 | unit |

The total TLFC gravity load for this study is 110.3 tons. This load is considered ***constant*** in all of our calculations in this paper. The variation of the draft is mainly caused by tendon tension. At the beginning of the analysis, where the TLFC is set to a free-floating condition, we calculate the equilibrium free-floating draft. The result is 3.5 m, as shown in Table 2. Then the designated draft is gradually increased until the maximum draft of 5 m is achieved. The higher the draft means higher tendon tension forces needed to apply the additional draft.

Table 4. TLFC Gravity Load

| Description | Weight (tons) |
|---|---|
| Topside station structures | 2.0 |
| Fishing gears | 2.4 |
| Ecotourism and research equipment | 3.1 |
| Mechanical of electrical instrumentation and plumbing | 2.1 |
| Total live load | 9.2 |
| Deck load total | 18.8 |
| Steel framing | 3.3 |

| Description | Weight (tons) |
|---|---|
| Wood flooring | 2.1 |
| Submerged net static load | 3.7 |
| Deck Structure Loads | 9.1 |
| Pontoon and Column Structure Self Weight | 7.40 |
| Fish stock weight [8] | 80 |
| **Total Gravity Load ( tons)** | **110.3** |

## 4. TLFC SURGE MOTION ANALYSIS

### 4.1 TLFC Displacement and Added Mass

The TLFC Displacement is calculated according to the draft variation. The following equation calculates the displacement:

$$\Delta = \rho\left\{4\left((l \times b \times h)\right)_{pontoon} + 4\left(\pi\left(\frac{D}{2}\right)^2 \times (T + \Delta T)\right)_{column}\right\} \quad (2)$$

Where:

$\Delta$ : TLP Displacement (tons)
$\rho$ : Seawater density (1.025 tons/m$^3$)
$\left((l \times b \times h)\right)_{pontoon}$ : Pontoon volume (Length × Breadth × Height) (m$^3$)
$\Delta T$ : Changes in draft
$\left(\pi\left(\frac{D}{2}\right)^2 \times (T + \Delta L)\right)_{column}$ : Column Sectional Area × (Draft+changes) (m$^3$)

The added mass varies with the change of the draft. TLFC column added mass could be acquired by following equation [13]:

$$m_{a\ column} = C_{A\ cyl} \times \rho \times V_{disp(column)} \quad (3)$$

The added mass coefficient is recommended by DNV RP-H103 [14]. In this case study, the added mass coefficient for the TLFC column is 0.703. Hereafter, we calculate added mass for TLP Column. The calculation of the added mass of the column is described in the following equation [13]:

$$m_{a\ ponton\ x} = \int_0^l (C_{A\ pontoon} \times \rho\pi a^2)\, dx \quad (4)$$

Where:

$m_{a\ pontoon\ x}$ : Pontoon added mass in surge motion (ton)
$m_{a\ column}$ : Column added mass (ton)
$C_{A\ pontoon\ X}$ : Added mass coefficient for pontoon in surge motion
$C_{A\ cyl}$ : Added mass coefficient for the column in surge motion
$V_{disp(column)}$ : Column displaced volume (m$^3$)
$\rho$ : Seawater density (1.025 ton/m$^3$)
$a$ : Pontoon length in surge motion direction

The total mass for dynamic calculation consists of displacement and added mass. The displacement, the added mass, and the total mass for each draft variation are displayed in Figure 6 below. It can be seen that the added mass of the pontoon is constant in the varied draft. This phenomenon can be clearly described by examining Equation 4, that there is no displacement function in the equation, and all the pontoons are fully submerged. Hence, there is no correlation between draft variation and the added mass of the pontoon in surge motion. The added mass of the column increases with the draft, displacement, and total mass. However, this study shows that the highest contributor to total mass is the pontoon's added mass. Even though the value is constant, the rectangular-shaped pontoon contributes more added mass than the tubular-shaped column.

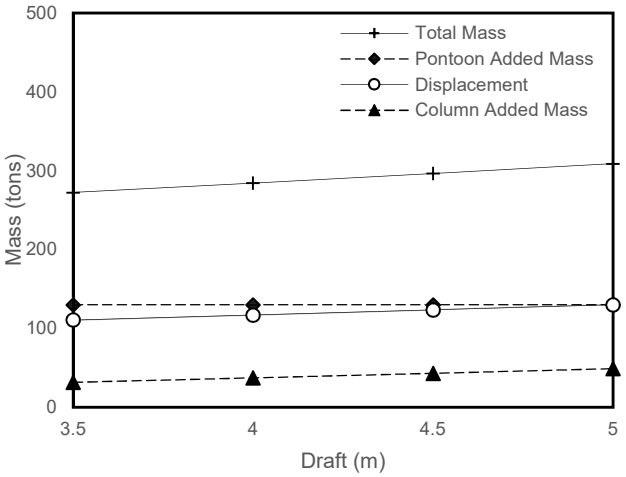


Figure 6. Displacement, added mass, and total mass in draft variation for surge motion.

### 4.2 Stiffness Calculation for Surge Motion

In this paper, an idealized tether stiffness model is used. This idealized stiffness is derived by assuming that each tendon is weightless and perfectly elastic with a known tension and elastic stiffness. The weightless cable is a straight line joining the two end coordinates. The resultant stiffness is evaluated assuming that the surface platform moves through small displacements relative to the cable lengths [10].

The difference between the buoyancy force from the floater and the predetermined floater draft generates the upward force and applies tension to the tendon ***$T_F$ (kN)*** (see Figure 7). When the excitation force encounters the floater and produces surge motion ***x (m),*** the tendon will produce restoring force ***$F_x$(kN/m).***

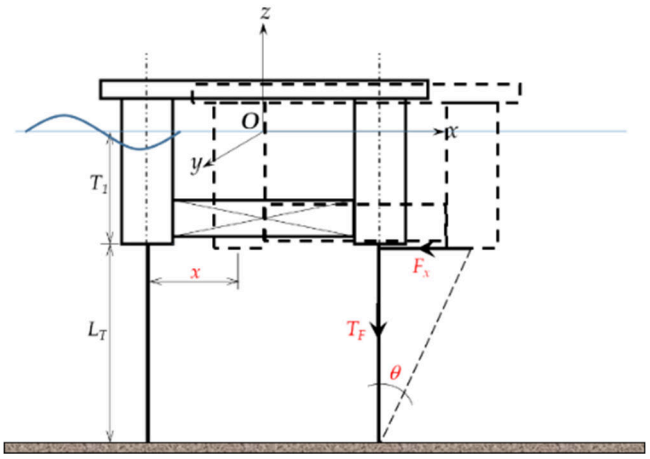


Figure 7. Tendon stiffness in surge motion

The tendon's restoring force can be determined as follows:

$$F_x = T_F \sin\theta \approx T_F \frac{x}{L_T} \quad (5)$$

$$F_x = \left(\frac{T_F}{L_T}\right) x \quad (6)$$

Equation 6 is a total of restoring force for surge motion. In the rigid body motion equation, we should generate the restoring coefficient, which is the force required to restore the body to its original equilibrium position per length unit [13]. Hence the surge stiffness coefficient is determined as follows:

$$k_x = \frac{T_F}{L_T} \quad (7)$$

Where:

$T_F$ : Tendon tension force (kN)
$L_T$ : Tendon length (m)

Each column has one tendon, so there are four total tendon members to form the TLFC tether system. Figure 8 below shows the tendon stiffness in various TLP drafts. It can be inferred that the stiffness linearly increases as the draft increases. The stiffness increases around 5.0 kN/m in every meter draft increase.

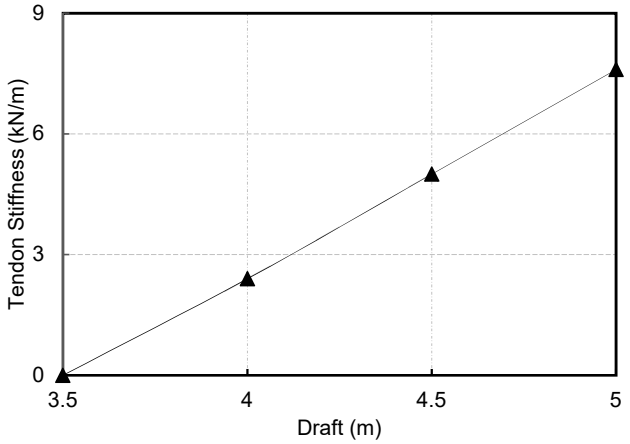


Figure 8. TLFC surge stiffness in varied Draft

### 4.3 Natural Period of Surge Motion

Surge natural frequency is calculated using equation (8), while equation (9) below describes the natural period.

$$\omega_{n\,Surge} = \sqrt{\frac{\mathrm{K_{Surge}}}{\mathrm{M + M_A}}} \quad (8)$$

$$T_{n\,Surge} = \frac{2\pi}{\omega_{n\,Surge}} \quad (9)$$

Where:

$\omega_{n\,Surge}$ : Surge natural frequency (rad/s)
$T_{n\,Surge}$ : Surge natural period (s)
$\mathrm{K_{Surge}}$ : Surge stiffness (kN/m)
$\mathrm{M + M_A}$ : Actual mass + added mass of surge motion (ton)

The natural period graph is described in Figure 9. The natural period tends to be shorter when the draft increases because of the increasing stiffness of the surge as the draft increases. The deeper the draft, the higher the tension generated by the tendon. The TLP natural period surge motion value in the draft of 3.5 m to 5.0 m is substantially far-off from the wave period, which generally occurs at 3 to 20 seconds.

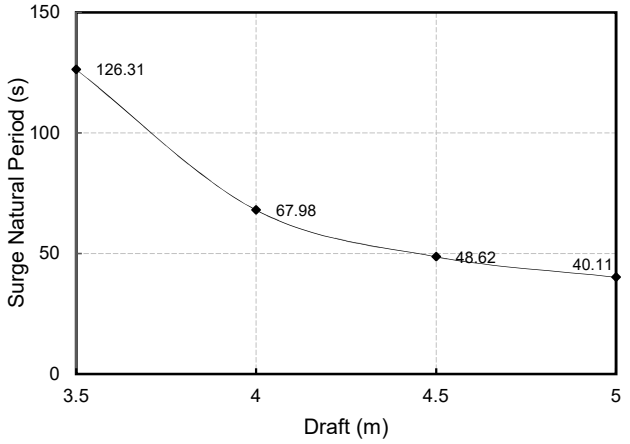


Figure 9. TLFC surge natural period

### 4.4 Excitation Force of Surge Motion

The calculation of the excitation force acting on the TLFC

floater structure consists of the acceleration force on the column and the pontoon. The equation for the force of the column and pontoon can be written as follows:

$$F_A^{column} = -M_{ax}^{column} \times \zeta_0 \times \omega^2 \cos(kx - \omega t) \int_{z0}^{z1} e^{kz} dz \quad (10)$$

$$F_A^{pontoon} = -M_{ax}^{pontoon} \times \zeta_0 \times \omega^2 \cos(kx - \omega t) \int_{z0}^{z1} e^{kz} dz \quad (11)$$

Where:

| | | |
|---|---|---|
| $F_A^{column}$ | : | Acceleration force acting on the column |
| $M_{ax}^{column}$ | : | Column added mass in surge motion |
| $\zeta_0$ | : | Wave amplitude = 1 m for RAO calculation |
| $\omega$ | : | Wave frequency (0.1 – 2.3 rad/s) |
| $k$ | : | Wave number |
| $x$ | : | Column and pontoon coordinate in the X axis |
| $\omega t$ | : | Wave phase (0 - 2 $\pi$) |
| $\int_{z0}^{z1} e^{kz} dz$ | : | Integration on the column and pontoon along its height from z0 (mean sea level = 0 m) to the structure's draft (-z m) |

We apply the excitation force using classic airy wave load to TLFC at a wave angular frequency of 0.1 to 2.3 rad/s. In Figure 10, we can examine the excitation force acting on the TLFC oscillates along with the wave frequency. The maximum excitation force occurs at a frequency of 1.1 rad/s with the value of, respectively, 363.24; 387.60; 420.73; 460.13 kN for 3.5; 4.0; 4.5; and 5.0 m draft. For every 1-meter increase in the draft, the force acting on the TLFC increases by an average of 20 percent.

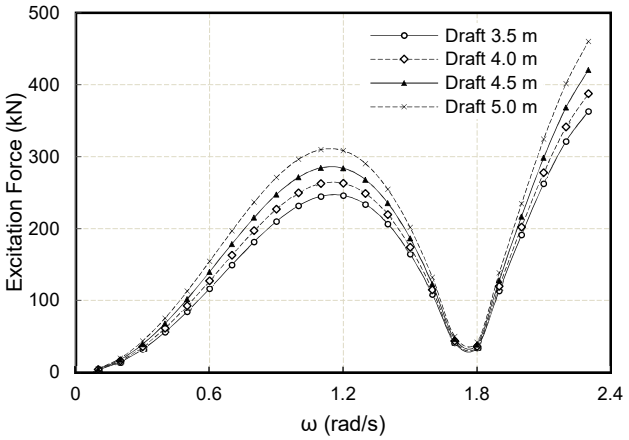


Figure 10. TLFC Wave excitation force for surge motion

### 4.5 Hydrodynamic Damping

The hydrodynamic damping $C_v$ in Equation 1 may be obtained from:

$$C_v = \pi c_f \left( \frac{F_0(\omega, \mu = 0)}{\zeta_0} \right)^2 \quad (12)$$

Where cf is the critical damping coefficient:

$$c_f = \frac{\omega^3 \cosh^2 kd}{4\pi\rho g^3 kd \tanh kd \left[1 + \frac{sin2kd}{2kd}\right]}$$

| | | |
|---|---|---|
| $\mu$ | : | Wave heading angle (degree) |
| $\zeta_0$ | : | Wave amplitude = $\frac{H_w}{2}$ |
| $\omega$ | : | Wave frequency (0.1 – 2.3 rad/s) |
| $\rho$ | : | Seawater density (1.025 ton/m$^3$) |
| $k$ | : | Wave number = $\frac{2\pi}{\lambda}$ |
| $d$ | : | Water depth (m) |

### 4.6 Response Amplitude Operator for Surge Motion (TLFC Response in Regular Unity Wave)

The TLP surge motion on regular waves can be analyzed through its Response Amplitude Operator (RAO). RAO is the amplitude of the surge motion to the wave amplitude ratio [15] and can be written as follows:

$$\text{RAO} = \frac{\zeta_x}{\zeta_0} = \frac{F_{0x}/K_x}{\sqrt{\left\{1 - \left(\frac{\omega}{\omega_n}\right)^2\right\}^2 + \{2c_f \frac{\omega}{\omega_n}\}^2}} \times \frac{1}{\zeta_0} \quad (13)$$

Where:

| | | |
|---|---|---|
| $\zeta_x$ | : | Surge motion amplitude (m) |
| $\zeta_0$ | : | Wave amplitude (RAO = 1 m) |
| $F_{0x}$ | : | Surge excitation force (kN) |
| $c_f$ | : | Damping coefficient |
| $K_x$ | : | Surge motion stiffness (kN/m) |
| $\frac{\omega}{\omega_n}$ | : | The ratio of wave frequency and TLP natural frequency |

Figure 12 shows the LTFC surge RAO (TLFC surge response in unity elevation regular wave). From the figure shown, TLFC has a high RAO value in the low-frequency region. The highest RAO value for draft 3.5, 4.0, 4.5 and 5.0 meters are respectively 1.38; 9.83; 2.59; 4.16 m/m. These phenomena can be explained by correlating them with each natural period in Figure 9. For draft 3.5 m, where no tendon tension is applied, the surge RAO gives a fairly low response with a maximum value of 1.38 m/m at a high-frequency wave. For a 4.0 m draft, with a surge of the natural frequency of 0.09 rad/s (67.98 seconds), the RAO value will be extremely high if there are waves near or similar periods. Resonance occurred at this draft at a wave frequency of 0.1 rad/s (63 seconds). With a one-meter wave load, the TLFC will respond with 9.83 m excitation. The same phenomenon occurs at 4.5 and 5.0 draft at an excitation wave frequency of 0.2 rad/s (31.45 seconds), although the response is not extreme as previously discussed. Indonesia luckily has a

mainly closed sea region with a wave period of 3 to 20 seconds, [16] hence the said resonances discussed above will not probably occur. We will examine further in this paper the spectral response in Section **Error! Reference source not found.**

## 5. TLFC Heave Motion Analysis

The TLFC displacement in heave motion is identical to its displacement in surge motion. Please refer to the displacement calculation in Section **Error! Reference source not found.**. The added mass of the TLFC column in heave motion is calculated using an equation of cylindrical tube added mass as described at [13], written as:

$$m_{Azc} = \frac{4}{3}\rho r^3 \quad (14)$$

While the added mass of TLFC pontoon in heave motion using rectangular volume as written below [13]:

$$m_{Azp} = C_A \times \rho\pi W^2 \times L \quad (15)$$

Where:

| | | |
|---|---|---|
| $m_{Azp}$ | : | Pontoon added mass in heave motion |
| $m_{Azc}$ | : | Column added mass in heave motion |
| $C_A$ | : | Added mass coefficient of rectangular volume in heave motion |
| $\rho$ | : | Seawater density (1.025 tons/m$^3$) |
| $r$ | : | Column radius (m) |
| $W$ | : | Pontoon width (m) |
| $L$ | : | Pontoon length (m) |

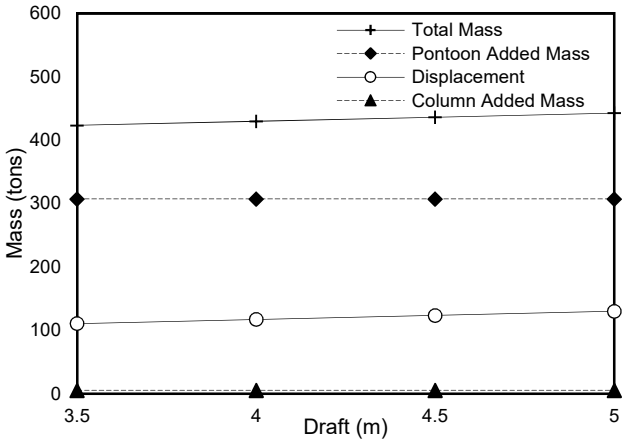


Figure 11. Displacement, added mass and total mass in draft variation for heave motion

Figure 11 shows the displacement, added mass, and total mass for each draft variation in heave motion. It can be inferred that all added mass for the column and pontoon are constant in various drafts. It is shown in Equations 14 and 15 that all the added mass equations do not involve any draft variation input—only the displacement increases along with the draft increase. For heave motion, like surge, the pontoon contributes more to total mass than the column.

### 5.1 Stiffness Calculation for Heave Motion

The stiffness of heave motion is caused by two factors: the hydrostatic stiffness of the floater waterplane area and the mechanical stiffness of the tendons. These two factors play an equally important role in restoring excessive heave motion. While the hydrostatic stiffness gives relatively 'tender' stiffness from its waterplane area, tendons give 'hard' stiffness rather than its mechanical properties. This mechanical stiffness is primarily affected by the material elastic modulus and the physical properties, namely length and sectional area. The heave motion stiffness can be obtained from [10]:

$$k_z = \rho g A_w + \frac{EA_T}{L_T} \quad (16)$$

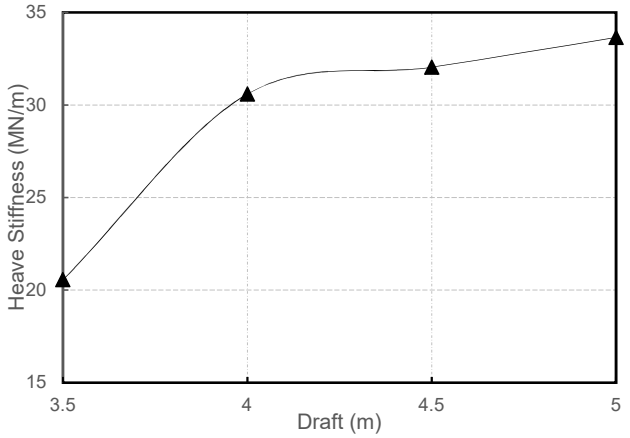


Figure 12. TLFC heave stiffness in varied draft

As shown in Figure 12 above, the stiffness of TLFC for heave motion is enormously high. The contribution of cable stiffness and the waterplane area create a highly stiff system in heave motion, typical to the TLP motion characteristics. We can see in Figure 13 the effect of high stiffness that creates an extremely low heave natural period.

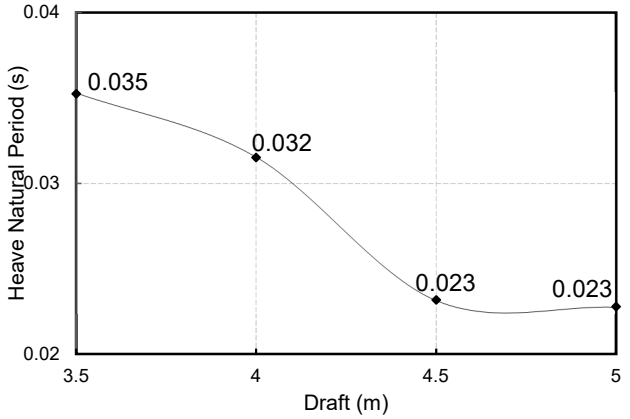


Figure 13. TLFC heave natural period.

### 5.2 Excitation Force of Heave Motion

The calculation of excitation force acting on the TLFC floater structure consists of the acceleration and pressure

force on the column and the pontoon. The pressure force for the column can be written as:

$$F_p^{col} = +\rho g \zeta_0 (\pi R^2) e^{kz} cos(kx - \omega t) \quad (17)$$

Furthermore, the pressure force for the pontoon is:

$$F_P^{Pon} = -\rho g \zeta_0 B e^{kz} \int_{-\frac{L}{2}}^{+\frac{L}{2}} \cos(kx - \omega t)\, dx \quad (18)$$

Meanwhile, the acceleration force for the column is described as follows:

$$F_A^{Col} = m_{az}^c \zeta_0 \omega^2 e^{kz}\, cos(kx - \omega t) \quad (19)$$

And the pressure force for the pontoon:

$$F_A^{Pon} = -m_{az}^p \zeta_0 \omega^2 e^{kz} \int_{-\frac{L}{2}}^{+\frac{L}{2}} \cos(kx - \omega t)\, dx \quad (20)$$

Where:

| | | |
|---|---|---|
| $F_a$ | : | Acceleration force acting on column and pontoon |
| $F_p$ | : | Acceleration force acting on column and pontoon |
| $m_{az}^c$ | : | Column added mass in heave motion |
| $m_{az}^p$ | : | Pontoon added mass in heave motion |
| $\zeta_0$ | : | Wave amplitude = 1 m for RAO calculation |
| $\omega$ | : | Wave frequency (0.1 – 2.3 rad/s) |
| $k$ | : | Wave number |
| $x$ | : | Column and pontoon coordinate in the X axis |
| $\omega t$ | : | Wave phase (0 - 4$\pi$) |

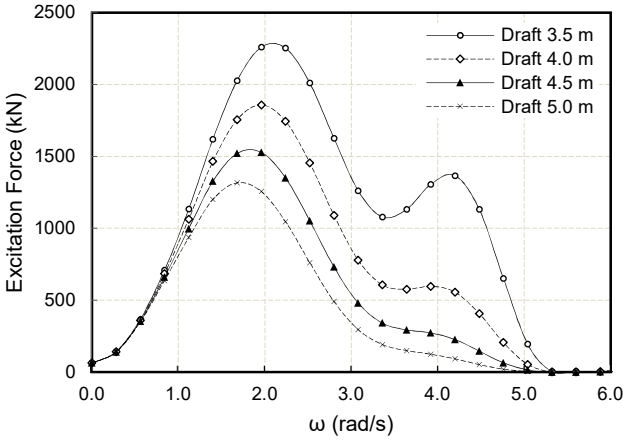


Figure 14. TLFC Wave excitation force for heave motion

Figure 14 above shows the wave excitation force for TLFC heave motion. We can see that the frequency range of TLFC heave motion is considerably higher than the surge motion. The excitation is due to the natural heave motion period located on the higher frequency waves and tends to stretch the range of the wave load. Also, [11] stated that the nature of the heave excitation force for the tension leg platform is in the high-frequency range. Therefore, the excitation force is considered small in low-frequency and wave-frequency regions. From the same graph, we can see that the increase in draft creates a lesser wave load. An increase in 1 m draft decreases an average of 16% of the maximum wave excitation force.

### 5.3 Response Amplitude Operator for Heave Motion

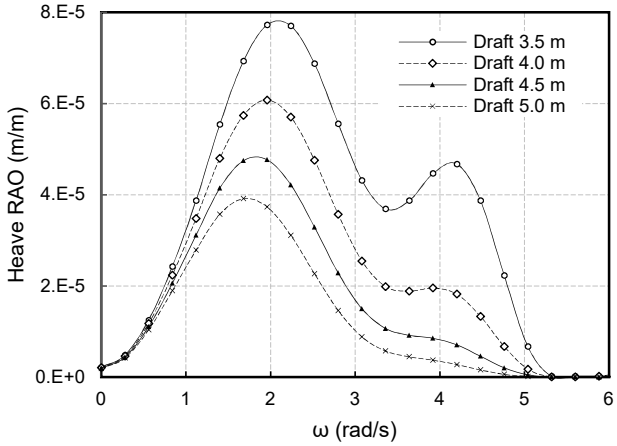


Figure 15. TLFC heave Response Amplitude Operator (RAO)

Figure 15 above shows the RAO for heave motion. Due to the enormous amount of heave stiffness, thanks to its tensioned tether configuration, the heave RAO in the wave frequency region is extremely small and can be considered negligible. The restricted heave motion will benefit the operation of the deck to support ecotourism and research activities. However, the high-frequency analysis should be further performed to assess the springing responses of the TLFC. This analysis is critical to determine the tendon fatigue calculation due to springing [9]. Further analysis of QTF (Quadratic Transfer Function) shall be in TLFC natural frequency as described in Figure 13, which is in the range of 160 to 280 rad/s (in the range of period from 0.022 to 0.04 second).

## 6. SPECTRAL RESPONSE (TLFC RESPONSE IN RANDOM WAVE)

This analysis is intended to determine the response characteristics of TLP motion in random waves. The motion response to random waves can be obtained by multiplying the RAO's squared value for each motion by the wave spectra. The wave spectra suitable for Indonesian waters are the JONSWAP wave spectra because of the archipelagic characteristics [17]. The JONSWAP spectra are based on experiments conducted in the North Sea. The JONSWAP

spectrum equation can be written by modifying the Pierson-Moskowitz [18] spectrum equation, namely:

$$S_j(\omega) = A_\gamma \, S_{pm}(\omega) \, \gamma^{\exp(-0.5\left(\frac{\omega-\omega_p}{\sigma\,\omega_p}\right)^2)} \quad (21)$$

There is another that is suitable for Indonesian waters, namely the ISSC wave spectra, and can be written as follows:

$$S_\zeta(\omega) = \frac{0{,}0081g^2}{\omega^5} \times \exp\left(\frac{-3{,}11}{H_s^2\omega^4}\right) \quad (22)$$

Where:

| | | |
|---|---|---|
| $S_j(\omega)$ | : | JONSWAP Spectra |
| $S_\zeta(\omega)$ | : | ISSC Spectra |
| $S_{pm}(\omega)$ | : | Pierson-Moskowitz spectra $\frac{5}{16} H_s^2\omega_p^4 \, \omega^{-5} \exp(-\frac{5}{4}\left(\frac{\omega}{\omega_p}\right)^{-4})$ |
| $\gamma$ | : | Peakness parameter |
| $\sigma$ | : | Shape parameter $\omega \leq \omega_0 = 0{,}07$ ; $\omega \geq \omega_0 = 0{,}09$ |
| $A_\gamma$ | : | normalizing factor = *1 – 0.287 ln*($\gamma$) |
| $\omega$ | : | wave frequency (rad/sec) |
| $\omega_p$ | : | angular spectral peak frequency (rad/sec) |
| $H_s$ | : | Significant wave height (m) |
| $Tp$ | : | Peak-to-peak wave period (s) |

Figure 16 below shows the result of the significant surge amplitude from JONSWAP and ISSC Spectra with significant wave height Hs varied from 1 to 10 m. The dotted graph shows the relationship between the amplitude increase in the surge motion amplitude and the increase in the significant wave height using ISSC Wave Spectra. While the continuous line graph shows the relationship between the significant surge amplitude and the increase in wave significant height using JONSWAP Wave Spectra. At Hs 1 to 2 meters, ISSC spectra have a lower value than JONSWAP spectra. However, at Hs more than 2 meters, the ISSC spectra characteristics have a considerably higher value than JONSWAP spectra. The further analysis shall be performed on the sea characteristics of the planned installation location of the TLFC.

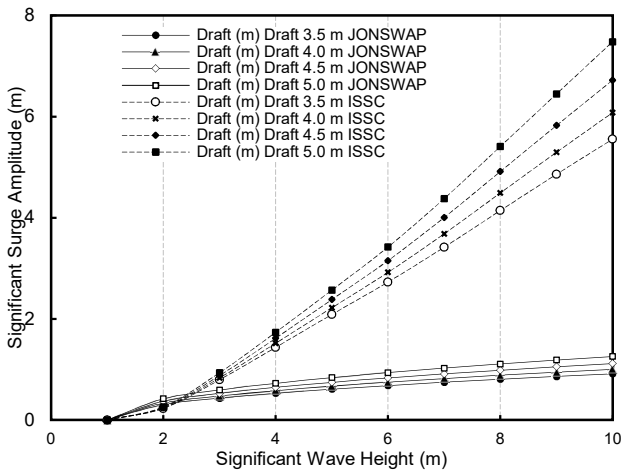


Figure 16. Significant surge amplitude vs. significant wave height

## 7. Conclusion

In this paper, we have demonstrated the analytical calculation method of TLFC response in surge and heave motion. The total mass is calculated by summarizing the actual displaced mass and the added mass due to the acceleration of the submerged TLFC floater structure. From the sensitivity study performed in this paper, it is concluded that the deeper the draft, the more added mass is created by the acceleration of the surge motion. For surge motion, the TLFC motion gets higher with the draft increase, despite the stiffness increase. This is caused by the further increase of the excitation force as the draft increases. The excitation force increases substantially higher than the stiffness on the tendon, as indicated by no reduction in TLP motion due to the increasing stiffness value. It is admitted that HDPE is a brittle material that cannot sustain any long period of constant tension. Hence the optimum tendon-floater connection for the structure is subject to further research.

## 8. References

[1] G. Merino *et al.*, “Can marine fisheries and aquaculture meet fish demand from a growing human population in a changing climate?,” *Glob. Environ. Chang.*, vol. 22, no. 4, pp. 795–806, Oct. 2012, doi: 10.1016/j.gloenvcha.2012.03.003.

[2] J. A. Hutchings and J. D. Reynolds, “Marine fish population collapses: Consequences for recovery and extinction risk,” *BioScience*, vol. 54, no. 4. American Institute of Biological Sciences, pp. 297–309, Apr. 01, 2004. doi: 10.1641/0006-3568(2004)054[0297:MFPCCF]2.0.CO;2.

[3] FAO, “Fishery and Aquaculture Country Profiles The Republic of Indonesia,” *Fishery and Aquaculture Country Profiles. Indonesia (2011). Country Profile Fact Sheets*, 2014. http://www.fao.org/fishery/facp/IDN/en (accessed Dec. 13, 2020).

[4] M. Heazle and J. G. Butcher, “Fisheries depletion

and the state in Indonesia: Towards a regional regulatory regime," *Mar. Policy*, vol. 31, no. 3, pp. 276–286, May 2007, doi: 10.1016/j.marpol.2006.08.006.

[5] D.H. Yusuf, R.S. Pahlevi, and P. Tambunan, "Report on a Regional Study and Workshop on the Environmental Assessment and Management of Aquaculture Development," 2015. http://www.fao.org/3/ac279e/AC279E13.htm (accessed Dec. 13, 2020).

[6] M. A. Iswara, "A land without farmers: Indonesia's agricultural conundrum," *13 Aug*, 2020. https://www.thejakartapost.com/longform/2020/08/13/a-land-without-farmers-indonesias-agricultural-conundrum.html (accessed Dec. 13, 2020).

[7] A. Lovatelli, J. Manjarrez, and D. Soto, *Expanding mariculture farther offshore*, no. 24. 2010.

[8] Y. I. Chu, C. M. Wang, J. C. Park, and P. F. Lader, "Review of cage and containment tank designs for offshore fish farming," *Aquaculture*, vol. 519. Elsevier B.V., p. 734928, Mar. 30, 2020. doi: 10.1016/j.aquaculture.2020.734928.

[9] Det Norske Veritas, *DNV-OS-C105 Structural Design of TLPs (LRFD Method)*, no. January. Det Norske Veritas, 2001.

[10] M. H. Patel and J. A. Witz, *Compliant Offshore Structure*, 1st Editio. Oxford: Butterworth-Heinemann Ltd, 1991.

[11] M. H. Patel, "Fluid loading on offshore structures," in *Dynamics of Offshore Structures*, Elsevier, 1989, pp. 174–214. doi: 10.1016/b978-0-408-01074-0.50008-2.

[12] J. M. Kapetsky, J. Aguilar-Manjarrez, and J. Jenness, "A global assessment of offshore mariculture potential from a spatial perspective," *FAO Fish. Aquac. Tech. Pap.*, p. 181, 2013.

[13] T. "Sarp" Sarpkaya, *Wave Forces on Offshore Structures*. Cambridge University Press, 2010. doi: 10.1017/CBO9781139195898.

[14] Det Norske Veritas, *DNV-RP-H103 Modelling and Analysis of Marine Operations*, no. April. Hovik, Norway: Det Norske Veritas, 2011.

[15] S. Chandrasekaran, *Dynamic Analysis and Design of Offshore Structures . Ocean Engineering & Oceanography.*, vol. 9. Chennai: Springer india, 2018. doi: 10.1007/978-981-10-6089-2.

[16] A. Toffoli and E. M. Bitner-Gregersen, "Types of Ocean Surface Waves, Wave Classification," in *Encyclopedia of Maritime and Offshore Engineering*, John Wiley & Sons, Ltd, 2017, pp. 1–8. doi: https://doi.org/10.1002/9781118476406.emoe077.

[17] D. Adrianto, E. B. Djatmiko, and Suntoyo, "The improvement of ultrasonic sensor-based device for direct ocean wave measurement program at Western Java Sea-Indonesia," *IOP Conf. Ser. Earth Environ. Sci.*, vol. 389, no. 1, 2019, doi: 10.1088/1755-1315/389/1/012022.

[18] DNVGLND, *DNVGL-ST-N001-Marine-Operations - Det Norske Veritas*. 2016.